Toxicology Reports 8 (2021) 1428–1436

Contents lists available at ScienceDirect

Toxicology Reports

journal homepage: www.elsevier.com/locate/toxrep

Self Nano-Emulsifying Curcumin (SNEC30) attenuates arsenic-induced cell death in mice

Zarqua Jamal [a], Joydeep Das [a], Payal Gupta [b], Pubali Dhar [c], Sreya Chattopadhyay [b], Urmi Chatterji [a,d,*]

[a] Cancer Research Laboratory, Department of Zoology, University of Calcutta, 35 Ballygunge Circular Road, Kolkata, 700 019, India
[b] Department of Physiology, University of Calcutta, 92 Acharya Prafulla Chandra Road, Kolkata, 700 009, India
[c] Laboratory of Food Science and Technology, Food and Nutrition Division, University of Calcutta, 20 B Judges Court Road, Alipore, Kolkata, 700027, India
[d] Centre for Research in Nanoscience and Nanotechnology, Technology Campus, University of Calcutta, JD-2 Sector III, Salt Lake City, Kolkata, 700 098, India

ARTICLE INFO

Handling Editor: Dr. Aristidis Tsatsakis

Keywords:
Arsenic
Self Nano-Emulsifying Curcumin (SNEC30)
ROS
Autophagy
Apoptosis
Anti-oxidant

ABSTRACT

Several precedents have confirmed numerous infirmities caused by arsenic poisoning, including immune suppression and cancer. Exposure to arsenic leads to alterations of the cellular machinery and eventually cell death, depending on the dose and duration of exposure. Oxidative stress induced by arsenic is the major mechanism by which it inflicts cellular toxicity, challenging the survival-support - autophagy and culminating in apoptosis in the thymus and spleen of mice. Curcumin, a potent dietary anti-oxidant with known anti-apoptotic and anti-inflammatory properties, was assessed for therapeutic benefits. However, the major caveat of this polyphenol is its low water solubility and limited bioavailability. Therefore, Self Nano-Emulsifying Curcumin (SNEC30) was used to treat mice exposed to arsenic. When administered, SNEC30 effectively ameliorated the adverse effects of arsenic in mice, by restoring structural alterations and reducing ROS-mediated cell death, thereby endorsing the importance of nutraceuticals in counteracting heavy metal-induced cellular toxicity.

1. Introduction

Toxicity due to heavy metals is a major problem and claims numerous lives worldwide, since they are stable and bio-accumulative within cells [1]. In recent years, increasing ecological and worldwide public health concern regarding environmental contamination by heavy metals has drawn a great deal of attention. Most importantly, deleterious upshots induced by heavy metals are insidious hazards leading to irreversible health effects and unfavorable outcomes [2]. Such contamination may occur as a result of industrial exposure, air effluence and water pollution. Several studies have shown that one such heavy metal, arsenic, induces apoptosis in many cell types from different organs, including skin, immune organs, reproductive organs, liver, and neuronal cells, and can disrupt the physiological homeostasis in exposed organisms [3–6]. Moreover, with the aid of ongoing research, it has become increasingly lucid that there are important dose-, time-, and tissue-specific differences in the effects of inorganic arsenic III compounds, as well as important gene-environment and co-exposure interactions, which determine how arsenic alters disease risk under a particular exposure circumstance [7–11]. Toxicity of arsenic is also dependent on the valency of arsenic. Inorganic trivalent arsenic poses to be far more toxic than pentavalent organic arsenic. Toxicity incurred by this group of compounds is largely due to the inhibition of pyruvate dehydrogenase, culminating in a reduced activity of the citric acid cycle and production of cellular ATP. Trivalent arsenic has high affinity for sulfhydryl moieties and therefore leads to inhibition of other cellular enzymes through sulfhydryl group binding [12]. Arsenate, on the other hand, acts as an analog of phosphate that competes for phosphate transporters in glycolytic and cellular respiration pathways leading to the uncoupling of oxidative phosphorylation. Organic arsenic is mostly common in seafood as arsenobetaine and arsenocholine, which are non-toxic compounds [13]. Although, it has become a general notion that organic arsenic is harmless, recent findings have proved that some organic arsenic compounds are as toxic as inorganic arsenic [14].

Earlier studies in our lab have shown that arsenic leads to various toxicities to the reproductive and immune organs, primarily by ROS generation and accumulative oxidative stress [3,6]. Since arsenic-induced immune modulation and cell death can severely affect

* Corresponding author at: Cancer Research Laboratory, Department of Zoology, University of Calcutta, 35 Ballygunge Circular Road, Kolkata, 700 019, India.
E-mail address: urmichatterji@gmail.com (U. Chatterji).

https://doi.org/10.1016/j.toxrep.2021.07.010
Received 19 January 2021; Received in revised form 17 March 2021; Accepted 15 July 2021
Available online 17 July 2021

normal physiological functioning, it was imperative to investigate possible therapeutic alternatives to counteract the stress.

Cellular damage by heavy metals is a persisting predicament for which no safe and effective therapy is available till date. Several prescribed drugs are banned regularly due to their severe side effects. Effective treatment approaches to tackle this problem are lacking; hence, novel strategies need to be adopted to defy the arsenic calamity. In recent years, herbal products have gained increasing interest to combat heavy metal poisoning because of their non-toxic and effective anti-oxidative properties [15]. Amongst such products curcumin, a hydrophobic polyphenol derived from the rhizome of the herb *Curcuma longa* [16], is widely known for its anti-inflammatory and antioxidant properties [17,18]. In addition, curcumin also exhibits anti-tumor, analgesic, immunostimulant, antiviral, antibacterial and antifungal properties. The chief components of this phytochemical include flavonoids and volatile compounds, such as tumerone, atlantone, and zingiberone [18]. Curcumin can treat diseases, like diabetes, asthma, allergies, neurodegenerative diseases, arthritis and atherosclerosis. In addition, curcumin can potentially modify crucial pathways involved in inflammation and carcinogenesis [18]. Reports have associated curcumin with the amelioration of copper-induced neurodegenerative diseases in *D. melanogaster* [16]. Prevalent studies have also pointed towards the fact that curcumin can prove to be more active in conjunction with other antioxidants like resveratrol and gallic acid and the trio have been found to ameliorate glyoxal-induced damage to the renal cells [19].

Curcumin has been developed as a leading compound for formulating new chemotherapeutic agents for treatment of several ailments owing to its pharmacological safety [20,21]. Curcumin is also believed to possess anti-carcinogenic and pro-oxidant properties that render it competent for the treatment of numerous diseases, including pancreatic malignancy, multiple myeloma, colon carcinoma, dementia, Alzheimer's disease and psoriatic skin [22–24]. Curcumin counteracted the adverse effects of sodium arsenite (Na AsO_2) by inducing activities of antioxidant enzymes [25] and was effective in preventing DNA damage, cell injury and apoptosis [26]. However, studies over the past three decades have revealed that bioavailability of curcumin is severely curtailed by its low water solubility, poor absorption, restricted distribution and high excretion [27].

Numerous nano-formulations including liposomes, polymeric nanoparticles, micelles, nanogels, niosomes, cyclodextrins, dendrimers, silver nanoparticles, and solid lipids have been developed over time to resolve these limitations [28,29]. Curcumin-phospholipid complexes have also been designed to overcome the limitations of absorption [30]. In this study, Self Nano-Emulsifying Curcumin 30 mg (SNEC30), a patented formulation was used to ameliorate the deleterious effects of arsenic on the primary and secondary immune organs in mice. The formulation is prepared by dissolving curcumin in a lipid system which is converted into an emulsion in the stomach. This enables complete dissolution and rapid absorption of curcumin into the bloodstream, enabling immediate action against painful and inflammatory conditions ensuring relatively high bioavailability and stability. Since the effects of SNEC30 on arsenic-induced cell death have not been investigated till date, the present study attempts to substantiate an effective strategy for combating arsenic-induced toxicity in the thymus and spleen of mice.

2. Materials and methods

Chemicals and kits: Natrium-*meta*-arsenite ($NaAsO_2$) was obtained from Merck, Darmstadt, Germany; SNEC30 was obtained from Arbro Pharmaceuticals Pvt. Ltd. (US patent no: US8835509); Annexin-FITC Apoptosis Detection kit was purchased from Bio Legend, USA; Acridine Orange and DCFDA from Abcam, U.K. cleaved PARP, Akt, pAkt1 (T^{450}), mTOR antibodies were procured from Abcam. Beclin1, LC3, Bax, Bcl2, p53 and p-mTOR antibodies were procured from Santa Cruz Biotechnologies, USA. Secondary antibodies (anti-mouse and anti-rabbit) were obtained from Santa Cruz Biotechnologies. GSH, CAT, SOD, DTNB and pyrogallol were all obtained from Sigma-Aldrich, USA.

2.1. Animals

Male Swiss albino mice, aged 10 weeks weighing 25 g, were procured from licensed breeding houses and maintained under controlled conditions (25 ± 2 °C room temperature, 50 ± 15 % RH and normal photoperiod of 12 h dark and 12 h light) throughout the experiment. The animals were given sterile food pellets and water *ad libitum* and allowed to acclimatize to the laboratory environment for 7 days prior to commencement of the experiments. All animal experiments were conducted as per approval and guidelines of the Institutional Animal Ethical Committee, Government of India (Registration Number 885/ac/05/CPCSEA). Principles of Laboratory Animal Care (NIH Publication No 85-23, revised in 1985) as well as specific Indian Laws of Animal Protection (ILAP) were followed throughout the experimental schedule. All care was taken to minimize the number of animals used and their suffering.

2.2. Selection of optimum arsenic and curcumin dose

Sodium arsenite (Na AsO_2) was administered in drinking water for 7 days followed by SNEC30 treatment for 14 days. Mice were divided randomly into six groups, each containing six animals (n = 6). The groups were as follows: Group I (control group, received arsenic-free water), Group II (received 5 ppm arsenic in drinking water), Group III (received 300 ppm arsenic in drinking water), Group IV (received drinking water with SNEC30 alone), Group V (received 5 ppm of arsenic + SNEC30) and Group VI (received 300 ppm of arsenic + SNEC30). The doses of $NaAsO_2$ selected were based on previously published studies [31,32] and the optimal concentration found in ground water (5 ppm) of South and Southeast Asian Belt including India, Bangladesh, Nepal, Vietnam and China [33]. An acute lethal dose, *i.e.,* 300 ppm, was selected keeping in mind the accidental ingestion of insecticides or pesticides and exposures that usually occur to miners, smelters, among others [33]. SNEC30 emulsion was administered with drinking water at a dose of 0.5 mg/kg of body weight, as recommended by the manufacturer.

2.3. Tissue collection

After treatment with arsenic and SNEC30, mice were sacrificed by means of rapid cervical dislocation. Thymus and spleen of the mice were promptly removed, weighed in an electrical monopan balance (Lutron GM-300 P) and processed for all subsequent experiments.

2.4. Analytical characterization of SNEC30

The SNEC30 nanoemulsion used in this study was analytically characterized for its contents using HPLC (Agilent 1260 Infinity II series), Agilent Technologies Pvt. Ltd., India, equipped with computation software (Open lab CDS, Chemstation Edition), G7122A degasser, G7111A quaternary pump, G1528C manual injector, G7165A MWD detector and a proshell 120EC-C18, 4 μm (4.5 × 150 mm) column.

2.5. Emulsion structure visualization

Cryogenic scanning electron microscopy (Cryo-SEM; Zeiss EVO-18-Special edition, Germany) was used to study the microstructure of the nanoemulsion. 50 μL of the samples were initially frozen to -180 °C in liquid nitrogen and then fractured and etched at -110 °C inside a preparation chamber. The samples were then coated with a gold-palladium alloy at a temperature of -170 °C in a sputter coater (Quorum Q150TES) and then visualized with the help of a scanning electromicroscope (Zeiss EVO-18, Germany).

2.6. Histology and morphometric analysis

Spleen and thymus slices from control and treated animals were fixed in Bouin's fluid, dehydrated in graded alcohol (50–100 %) and embedded in paraffin. Thin sections (5 μm) were stained with routine hematoxylin-eosin stain for photo-microscopic assessment [9] under a light microscope (Dewinter Optical Inc., India). The stained sections were subjected to morphometric analysis using the Dewinter Caliper Pro software (Vers. 4.1).

2.7. Scanning electron microscopy

Spleen and thymus were dissected and fixed overnight in 2.5 % glutaraldehyde with 0.2 M phosphate buffer at 4 °C. Fixed tissues were washed and subsequently dehydrated through ascending grades of ethanol, placed in chilled acetone, and air dried, overnight [3]. After critical point drying, the tissues were coated with gold-palladium in a sputter coater (Quorum Q150TES) and finally viewed by SEM (Zeiss EVO-18-Special edition, Germany); [3].

2.8. Single cell suspension

Thymus and spleen obtained from the sacrificed mice were washed in PBS and gently tapped with sterile blunt ended forceps. The single cells were sieved with the help of nylon mesh (pore size 40 μm) and washed three times with PBS. Cells were then counted and 1×10^6/mL cell suspensions were used for the experiments [34].

2.9. Estimation of intracellular ROS generation

ROS generation in the thymus and spleen of arsenic, arsenic + SNEC30 and SNEC30 only exposed mice was measured using the oxidation sensitive fluorescence probe, 2′,7′-dichlorodihydroflurescein diacetate (DCFDA, Abcam). In presence of ROS, DCFDA is oxidized to form a fluorescent compound 2′,7′-dichlorofluorescein (DCF). 20 μM DCFDA were added to the cell suspension prepared from the thymus and spleen of the experimental groups and incubated for 30 min at 37 °C in the dark [3]. DCF fluorescence was detected by a FACS scan flow cytometer (BD FACS VERSE, USA) at 530 nm and was analyzed by the BD FACSuite™software.

2.10. Estimation of ROS scavenging enzymes

2.10.1. Preparation of post-mitochondrial supernatant (PMS)

Thymus and spleen, procured from the experimental animals were homogenized in 0.1 M PBS with KCl (1.17 % w/v) and centrifuged at 800 G for 5 min at 4 °C to separate the nuclear debris. The supernatant obtained was re-centrifuged at 10,500 G for 20 min to obtain the post mitochondrial fraction [34].

Reduced glutathione (GSH) content of thymocytes and splenocytes was determined from protein-free filtrate of thymic post-mitochondrial supernatant (PMS) based on the reduction of 5,5′-dithio-bis-(2-nitrobenzoic acid) (DTNB) at 412 nm, by the method of [35]. GSH content was measured from a standard curve, and expressed in μM/mg protein.

Catalase (CAT) activity in thymocytes and splenocytes was evaluated spectrophotometrically from thymic and splenic PMS, based on the method described by Claiborne [36]. Decomposition of H_2O_2 to H_2O and O_2 by CAT present in the protein-free filtrate at 240 nm was expressed as μM of H_2O_2 U/mg of protein.

Superoxide dismutase (SOD) activity was assayed from the cell lysates of thymocytes and splenocytes following the method described by Marklund and Marklund [37], based on the auto-oxidation rate of pyrogallol at 420 nm and inhibition of this auto-oxidation by SOD where 50 % inhibition corresponded to one unit of enzyme activity. Activity was expressed as units/mg of protein.

2.11. Detection of acidic vesicles

Acridine orange (1 mg/mL) was added to untreated as well as treated cells for 15 min at 37 °C. Next, cells were washed twice with PBS. Images of cells were obtained using Olympus laser-scanning confocal microscope (FV-10 ASW 3.0 viewer image browser) at 450 nm and 593 nm for the detection of acidic vesicular organelles [3].

2.12. Analysis of apoptotic cells by flow cytometry

Cells (1×10^6) from thymus and spleen of control, arsenic and curcumin-exposed mice (n = 6) were collected and stained with Annexin V-FITC and propidium iodide (PI). Cells were eventually analyzed on a flow cytometer (BD ACCURI, BD Biosciences, USA) and analyzed by BD ACCURI C6 software (Vers. 1.0.264.21). The experiment was performed in triplicate for statistical significance [3].

2.13. Immunoblotting

Cells were washed and lysed in ice-cold RIPA cell lysis buffer (150 mM NaCl, 50 mm Tris, 0.1 % Triton X-100 and 0.1 % sodium dodecyl sulphate (SDS) containing protease inhibitors [4-(-2-aminoethyl) benzenesulphonyl fluoride], EDTA, leupeptin, aprotinin and bestatin, SIGMA). Protein concentration was determined using the Bradford assay. Proteins were resolved by SDS-polyacrylamide gel electrophoresis and transferred onto nitrocellulose membranes. The membranes were subsequently probed with primary antibodies against p53, Bax, Bcl-2, LC3, Beclin-1, cleaved-caspase 3, cleaved-PARP, Akt, p-Akt, mTOR and p-mTOR overnight at 4 °C. Antibody to β-tubulin was used as loading control. After incubation with horseradish peroxidase-conjugated secondary antibodies, antibody binding was assessed by using enhanced chemiluminescence. Bands were quantified using Image J software (Vers. 1.46r) [3].

2.14. Statistical analysis

Results of the experiments, performed in triplicates (n = 6), were expressed as mean ± standard error, using a statistical software package (Graphpad Prism, Vers. 6.0). Each arsenic treated group was compared to the control and the differences between the group mean values were evaluated by Student's *t*-test as all data sets were normally distributed; *p*-values less than 0.05 were considered statistically significant.

3. Results

3.1. Characterization of curcuminoid nanoemulsion

In order to determine the purity of the nanoemulsion and ensure that its contents would enter the cells of the thymus and spleen, HPLC was used to identify and quantify the three curcuminoids, *viz.*, curcumin, demethoxycurcumin and bismethoxycurcumin in SNEC30. Fig. 1A provides the sample information and Fig. 1A (table) shows the retention time obtained from the experiment which positively identifies all three curcuminoids compared to the standard run. Based on the regression lines obtained from the standard curve, the percentage area under the peak reflecting the concentration of each component was recorded. The data shows that the SNEC30 nanoemulsion contains 80.26 % curcumin, 17.86 % demethoxycurcumin and 1.88 % bis-demethoxycurcumin (Fig. 1A, table). The cryo-SEM micrographs revealed multiple frozen droplets of the nanoemulsion, with particle diameter ranging from 25 nm to 250 nm. It was also noted that the particles formed aggregates upon being frozen (Fig. 1B).

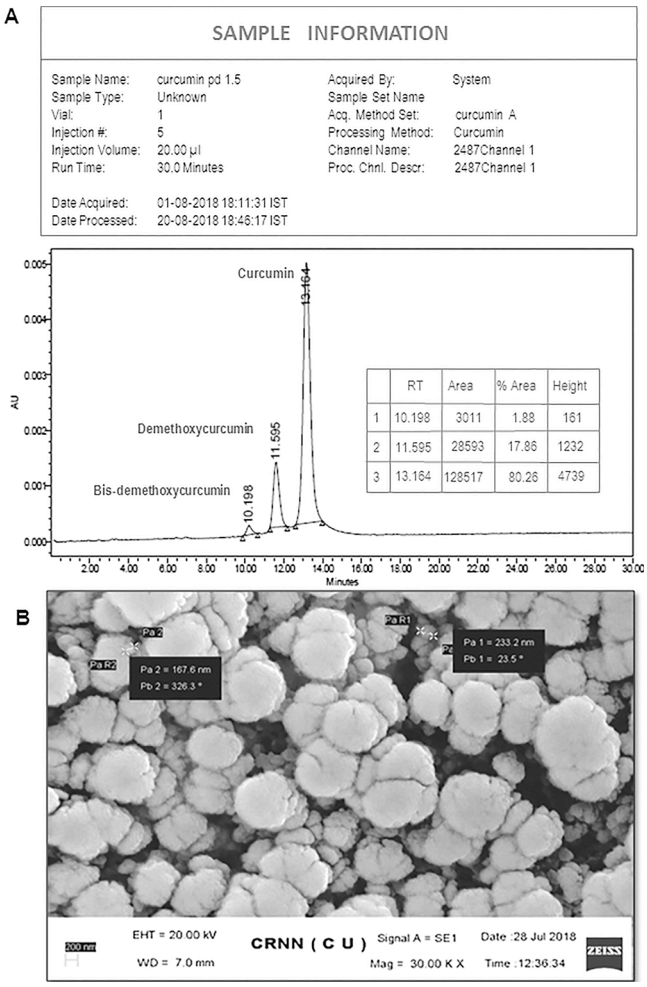

Fig. 1. Characterization of SNEC30. (A) HPLC chromatogram of curcumin nanoemulsion by employing Agilent 1260, Infinity II series HPLC. A gradient system of 1 % formic acid in acetonitrile, 60/40 v/v was used (λ_{max} 424 nm). The peak time of curcumin, demethoxycurcumin and bisdemethoxycurcumin was 13.164, 11.595 and 10.198 min. **(B)** SEM micrograph of SNEC30 nanoemulsion, showing particle size to be in the range of 25-250 nm. Images are at 30,000×; bar, 200 nm.

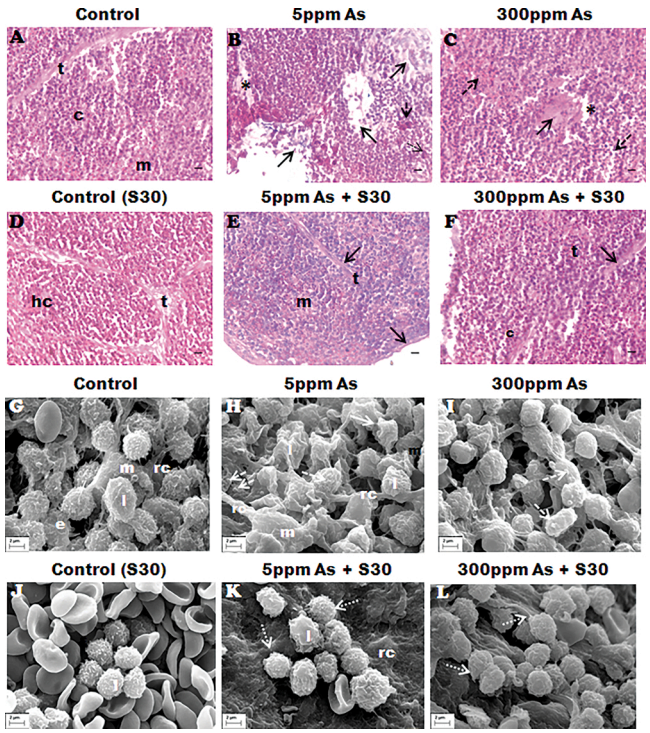

Fig. 2. Effect of SNEC30 treatment on the tissue architecture of arsenic-exposed mice thymus. Mice (n = 6) exposed to arsenic for 7 days were treated with SNEC30+As for 14 days. Arsenic-treated sections **(B and C)**, showed a significant decrease in cellularity as compared to the untreated one **(A)**. Broken arrows indicate pyknotic nuclei; solid arrows indicate loss of cells; asterisks indicate dilated sinusoids. **(D)** Section from mice treated with SNEC30, depicting normal histology. Arrows mark partial recovery in terms of organization and tissue architecture in sections treated simultaneously with SNEC30 along with arsenic for 14 days **(E and F)**; c, cortex; m, medulla; t, trabaculae, hc, Hassal's corpuscle; magnification 40×; scale bar 10 µm. **(G-L)** represent the ultra structural images of thymus by scanning electron microscopy at a magnification of 10,000×; scale bar 2 µm. **(G)** Micrograph of control thymus depicting normal surface morphology. Loss of microprocesses from lymphocytes are marked by arrows, broken arrows indicate cell-membrane blebs **(H and I)**. **(J)** Micrograph of SNEC30 treated thymus, depicting normal features. Dotted arrows indicate restoration of the surface morphology of the tissue upon treatment with SNEC30 **(K and L)**; l, lymphocytes; rc, reticular cells; e, epithelial cells; m, macrophages.

3.2. SNEC30 restores arsenic-induced histopathological alterations in the thymus and spleen

Histological analyses of the thymic sections of arsenic treated mice compared to that of untreated mice (Supplementary Fig. 1; Fig. 2A), depicted significant alterations in morphology of 5 and 300 ppm treatment groups (Fig. 2B and C). Areas of lymphocyte depletion (marked by solid arrows, Fig. 2B) were evident. Loss of cortico-medullary demarcation and dilated sinusoids (indicated by asterisks) were also observed (Fig. 2B and C). Accumulation of apoptotic bodies (pointed by broken arrows) increased by 6- and 8.3-fold ($p < 0.001$), (Fig. 2B and C). Capsular disintegration and loss of trabecular structures were evident (Fig. 2B and C). Thymus histology of 300 ppm group revealed inflammation marked by eosinophil stained area, indicated by solid arrow (Fig. 2C). Administration of SNEC30 after arsenic exposure ameliorated the aforesaid degenerative effects of arsenic on the thymus (Fig. 2D). There was a marked reduction in the scores of apoptotic bodies (3.7- and 3.36-fold, respectively; $p < 0.001$) in the 5 ppm+SNEC30 and 300 ppm+SNEC30 groups compared to the 5 and 300 ppm arsenic-only treated groups. The sinusoids formed due to arsenic exposure were seen to regenerate and inflammation caused was healed (Fig. 2E and F). Reformation of trabeculae and capsule was also observed.

Scanning electron microscopic studies revealed a decrease in the size of thymocytes of 5 ppm (1.3 folds; $p < 0.05$) and 300 ppm (1.7 folds; $p < 0.01$) compared to the control (Fig. 2G), loss of interlobular septae, an increase in surface irregularities and loss of homogeneity and compactness in the structural organization of the tissues in the arsenic-treated groups (Fig. 2H and I) were found. Additionally, distinct protrusions simulating membrane blebbing (indicated by broken arrows), a definitive indication of apoptosis, was observed (Fig. 2H and I). Loss in cellular receptors was common in both 5 and 300 ppm of arsenic treated groups (Fig. 2H and I). Thymocytes of animals treated with SNEC30 alone resembled those of the untreated mice (Fig. 2J). Normal spherical structures of the cells were restored and compactness was revived in 5 ppm + SNEC30 group and 300 ppm + SNEC30 group compared to 5 and 300 ppm arsenic-treated groups. Membrane blebbing was reduced and surface receptors (marked by dotted arrows) were seen to reform (Fig. 2K and L).

The spleen of the arsenic-treated animals was also severely affected (Supplementary Fig. 2). Compared to the control (Fig. 3A), histological and morphometric results demonstrated an increase in the red pulp area of 5 ppm (1.3-fold; $p < 0.05$), as well as, 300 ppm groups (3.6-fold; $p < 0.001$). The tissues appeared to be congested with hemolyzed blood cells

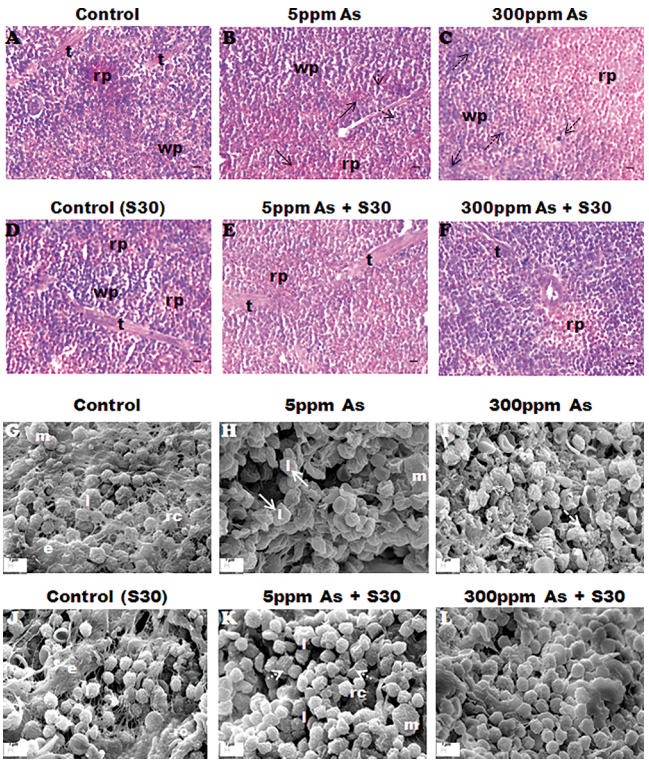

Fig. 3. Ameliorative effects of SNEC30 on arsenic-induced spleen injury. Histopathological evaluation of arsenic-exposed mice (n = 6) spleen was performed by means of standard H&E staining. **(A)** Control mice spleen section, showing normal tissue architecture. **(B and C)** Arsenic intoxicated mice spleen sections, illustrating expansion in red pulp area, tingible bodies marked by arrows and pyknotic nuclei marked by broken arrows. **(D)** Section of spleen from mice treated with SNEC30 for 14 days, depicting intact histological structure. **(E and F)** Sections of spleen treated with arsenic followed by SNEC30 nanoemulsion + As, depicting marked reduction in the red pulp area and the restoration of tissue histology back to normalcy; wp, white pulp; rp, red pulp; t, trabaculae, c, capsule; magnification 40×; scale bar 10 μm. **(G–L)** SEM micrographs of spleen at a magnification of 5000 × . **(G)** Micrograph of control spleen with normal structural integrity. **(H)** Solid arrows indicate splenocytes with increased diameters in 5 ppm arsenic treated group and broken arrows mark blebbing of cellular membrane, indicative of apoptotic cells in 300 ppm group **(I)**. **(J)** Micrograph of SNEC30 treated spleen, depicting normal features. **(K and L)** SNEC30+As treated groups showing restoration of cellular size, shape and reduction in apoptosing cells. l, lymphocytes; m, macrophages; rc, reticular cells; e, epithelial cells; scale bar 1 μm (For interpretation of the references to colour in this figure legend, the reader is referred to the web version of this article).

in arsenic exposed groups. There was a decrease in the number of trabeculae. Many lymphocytes were observed with pyknotic nuclei (broken arrows; Fig. 3B and C). Upon treatment with curcumin nanoemulsion, the red pulp area reduced significantly in the 5 ppm + SNEC30 (1.3-fold; $p < 0.05$) and 300 ppm+SNEC30 (1.6-fold; $p < 0.01$) treated groups and the spleen was found to be reconstituted (Fig. 3E and F). Marked reduction in cells with pyknotic nuclei was observed, and was comparable to SNEC30 treated mice (Fig. 3D). Scanning electron microscopic studies revealed that compared to the control (Fig. 3G), an increase in the size of splenocytes of 5 ppm arsenic-treated group (1.8-fold; $p < 0.001$). Loss of interlobular septae, an increase in surface irregularities and loss of homogeneity and compactness in the structural organization of the tissues (Fig. 3H) was also observed. At the 300 ppm concentration, cell shrinkage and absolute disintegration of the integrity of the tissue was noted (Fig. 3I). Distinct protrusions simulating membrane blebbing (broken arrows) was also observed (Fig. 3I). Spleen of animals treated with SNEC30 alone resembled those of the control (Fig. 3J). Splenocytes of 5 ppm arsenic + SNEC30 group was seen to regain its normal size (dotted arrows) which was found to decrease by 1.6 fold ($p < 0.01$), compared to those of the 5 ppm arsenic treated group. Splenocytes of the 300 ppm arsenic+SNEC30 group depicted reduced membrane blebbing and the tissue was seen to regain compactness and integrity (Fig. 3K and L).

3.3. SNEC30 reinstates arsenic-induced redox imbalance in immune cells

It is well established that arsenic induces reactive oxygen species (ROS) generation, which is chiefly responsible for the disruptive effects on the immune organs. Subsequently, the level of DCF fluorescence was monitored using 2′,7′-dichlorodihydrofluorescein diacetate (DCFDA) for directly measuring the redox state of a cell. Generation of arsenic-induced intracellular ROS was clearly evident in the thymus of 5 ppm (1.5-fold; $p < 0.01$) and 300 ppm (2.1-fold; $p < 0.01$) groups (Fig. 4A and B) and in the spleen of 5 ppm (1.8 fold; $p < 0.01$) and 300 ppm (2.25 fold; $p < 0.001$) groups (Fig. 4F and G). After treatment with SNEC30, ROS generation was reduced significantly in the thymus by a 2-fold ($p <$

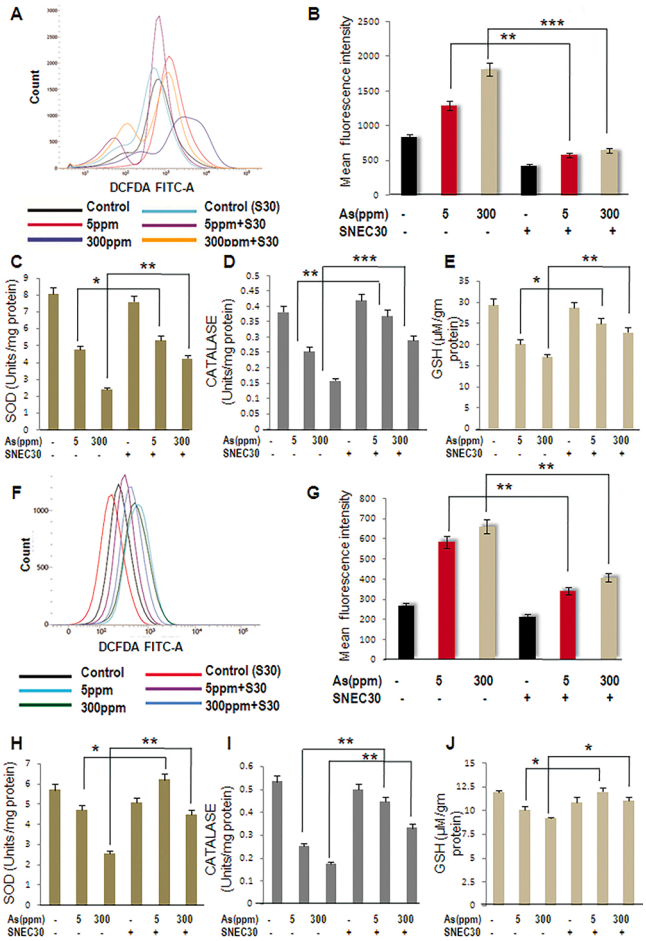

Fig. 4. Alterations in the levels of ROS in response to arsenic and SNEC30 treatment. Representative histogram profiles of DCF fluorescence of thymus **(A and B)** and spleen **(F and G)**. Figures illustrate a dose-dependent increase in ROS generation upon exposure to arsenic for 7 days. Treatment with SNEC30+As for 14 days following arsenic treatment counteracted the oxidative effects of arsenic and downregulated arsenic-induced ROS generation. Error bars represent S.D. from the mean of three independent experiments. **(C-E and H-J)** Depicts results of enzyme assays carried out for measuring the activities of ROS scavenging enzymes SOD, CAT and the level of reduced glutathione GSH in thymus and spleen of mice treated with only arsenic for 7 days and SNEC30+As for 14 days. Error bars represent S.D. from the mean of three independent experiments. *$p < 0.05$, **$p < 0.01$, ***$p < 0.001$.

0.01) and a 2.8-fold ($p < 0.001$) in the 5 ppm+SNEC30 and 300 ppm+SNEC30 exposed groups, respectively, as compared with the arsenic-treated animals (Fig. 4A and B) and by a 1.4-fold ($p < 0.05$) in the 5 ppm+SNEC30 and a 2.4-fold ($p < 0.01$) in the 300 ppm+SNEC30 treated groups of spleen (Fig. 4F and G), compared to the arsenic only-treated mice.

Since dose-dependent increase in ROS was observed, we subsequently investigated the activity of ROS scavenging enzymes, which are the key players of the endogenous defense system that combat the damage instituted by arsenic exposure. Our results indicated that arsenic led to considerable dose-dependent reduction in the activity of SOD, CAT and GSH of both the thymus and spleen (Fig. 4C–E and H–J). After treatment with SNEC30, significant restoration of the activity of SOD, CAT and GSH were noted (Table 1). The results collectively suggested that SNEC30 could attenuate $NaAsO_2$-induced oxidative stress.

3.4. *Effect of SNEC30 on arsenic-induced altered expression of autophagic markers of thymus and spleen*

Confocal imaging was carried out with cells of the respective tissues stained with acridine orange and representative micrographs of control, arsenic and arsenic + SNEC30-treated cells from thymus and spleen are shown in Fig. 5A and B. Both 5 ppm and 300 ppm arsenic treatments enhanced formation of autophagosomes in thymocytes and splenocytes ($p < 0.05$ and $p < 0.001$, respectively). Upon treatment with SNEC30, reduction in accumulation of acidic vesicles was observed in both the thymus (Fig. 5A) and spleen (Fig. 5B) of 5 ppm + SNEC30-treated mice, and was significant in the 300 ppm + SNEC30-treated mice ($p < 0.01$). To further establish the active involvement of autophagy in arsenic-mediated stress management, expression of the components of PI3K pathway regulating autophagy was investigated. Significant reduction in the expressions of PI3K, phospho-Akt and phospho-mTOR ($p < 0.001$) were observed in the thymus (Fig. 5C) and spleen (Fig. 5D). Concomitantly, enhanced expression of Beclin-1 and LC3-II ($p < 0.001$) further confirmed ensuing autophagy in the respective tissues following arsenic treatment. Treatment with SNEC30 revealed that arsenic-induced autophagy could be attenuated (Fig. 5C and D) and it was validated both by acridine orange staining (Fig. 5A and B) and western blot which showed a marked increase in the expressions of PI3 K, phospho-Akt and phospho-mTOR ($p < 0.01$) together with reduced expression of Beclin 1 and LC3-II in the thymus (Fig. 5C) and spleen (Fig. 5D), compared to the arsenic only treated groups.

Table 1
SOD, CAT and GSH levels of arsenic treated and arsenic as well as SNEC30 treated mice. One experimental set of mice was exposed to 5 ppm and 300 ppm sodium meta-arsenite for 7 days and another set was treated with arsenic for 7 days followed by 0.5 mg/kg BW. of SNEC30+arsenic (5 and 300 ppm) for 14 days. Arsenic exposure led to a significant decrease in SOD and CAT activities and caused a reduction in the levels of reduced GSH. Treatment with SNEC30 led to an improvement in the activities of the ROS scavenging enzymes SOD and CAT and an increase in GSH levels. The data shown is representative of experiments carried out in triplicates, $*p < 0.05$, $**p < 0.01$ and $***p < 0.001$ as compared with the control, for the first set; $*p < 0.05$, $**p < 0.01$ and $***p < 0.001$ as compared with respective arsenic only treated groups, for the second set. (For interpretation of the references to colour in this Table legend, the reader is referred to the web version of this article).

Organ/ AO Factor	5 ppm		300 ppm		5 ppm + SNEC 30		300 ppm + SNEC 30	
	Fold change	*P* value	Fold change	*P* value	Fold change	*P* value	Fold change	*P* value
Thymus **SOD**	2.2⇩	0.01	3.36⇩	0.001	1.47⇧	0.01	1.8⇧	0.01
Thymus **CAT**	1.5⇩	0.01	2.4⇩	0.001	1.5⇧	0.01	2.4⇧	0.001
Thymus **GSH**	1.45⇩	0.01	1.72⇩	0.01	1.25⇧	0.05	1.43⇧	0.01
Spleen **SOD**	1.2⇩	0.05	2.28⇩	0.001	1.3⇧	0.05	1.8⇧	0.01
Spleen **CAT**	2.12⇩	0.01	2.8⇩	0.001	1.76⇧	0.01	1.88⇧	0.01
Spleen **GSH**	1.2⇩	0.01	1.33⇩	0.01	1.2⇧	0.05	1.22⇧	0.05

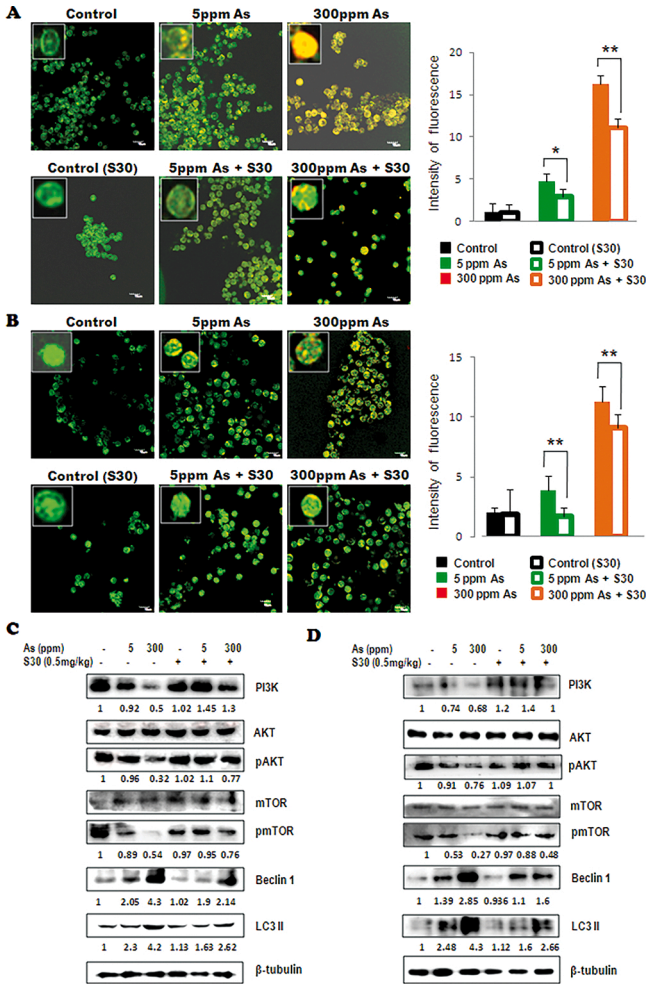

Fig. 5. Monitoring alterations in autophagy in thymus and spleen of Swiss-albino mice using SNEC30 after arsenic exposure. (A and B) Cellular autophagy in thymus **(A)** and spleen **(B)** measured by AO staining. The presence of acridine orange stained acidic vesicles in the thymus and spleen cells, visualized by confocal microscopy (scale bar 10 μm) confirmed autophagy upon arsenic exposure. With the administration of SNEC30, there was a decrease in the fluorescence intensity of the cells of thymus and spleen indicating towards a reduction in the acidic vesicular accumulation. The intensity of fluorescence in thymocytes and splenocytes of arsenic groups *versus* SNEC30+As groups was quantified (right panels), error bars represent S.D. from the mean of three independent experiments. $*p < 0.05$, $**p < 0.01$. **(C and D)** Western blots showing expression of autophagic protein markers in thymus **(C)** and spleen **(D)**. β-tubulin was used as loading control and respective fold changes are represented as ratio of net band pixel density of arsenic treated groups to the control. The data shown is a representative of the experiments carried out in triplicates.

3.5. *Effect of SNEC30 on arsenic-induced apoptotic death of immune cells*

As evaluated by Annexin V/PI assay, there were significantly more apoptotic cells in the thymus (Fig. 6A) and spleen (Fig. 6C) of the arsenic-exposed mice, as compared to the untreated mice ($p < 0.01$). Concomitantly, changes in apoptotic markers were observed in the thymus and spleen of 5 ppm and 300 ppm arsenic-treated groups over controls. A dose-dependent decrease in the expression of Bcl-2 ($p < 0.001$) and an increase in the expression of Bax ($p < 0.05$), cleaved Caspase 3 ($p < 0.01$) and cleaved PARP ($p < 0.001$) was observed (Fig. 6B and D). Interestingly, significantly increased expression of p53

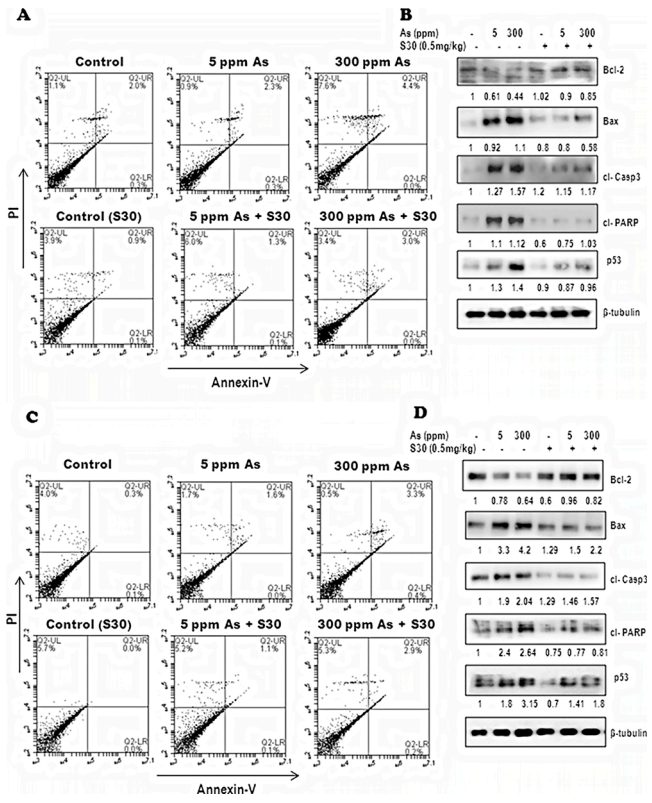

Fig. 6. SNEC30 attenuates arsenic-induced cell death in mouse thymus and spleen. (A and C) Quantified panels of Annexin V-FITC and PI double staining graphs obtained from the thymus **(A)** and spleen **(C)** of mice treated with sodium arsenite for 7 days followed by SNEC30+As treatment for 14 days. **(B and D)** Immunoblots of apoptotic protein markers from thymus **(B)** and spleen **(F)** of arsenic and SNEC30+As treated mice. β-tubulin was used as loading control and respective fold changes are represented as ratio of net band pixel density of arsenic and SNEC30+As treated groups to the control. Data are representative of three independent experiments carried out in triplicates.

($p < 0.001$), indicated that apoptosis in response to arsenic was p53-dependent. Treatment with SNEC30 reduced the number of apoptotic cells in

the thymus by a 2-fold ($p < 0.001$) and spleen by a 1.5-fold ($p < 0.05$) compared with mice treated with arsenic alone (Fig. 6A and C). In addition, the expressions of both pro- and anti-apoptotic markers were also observed to undergo restoration towards normal levels after treatment with SNEC30 (Fig. 6B and D).

4. Discussion

The involvement of the immune organs and association of the immune system in the regulation of arsenic-mediated toxicity has not been delineated till date. Given the fact that generation of ROS is the most distinct mechanism of arsenic toxicity, it was speculated that compounds having anti-oxidant property might be effective in combating arsenic toxicity. Numerous studies have confirmed that curcumin exerts extensive pharmacological actions in various diseases, including immune-suppression in mice, mostly by virtue of its antioxidant properties [38–40]. Curcumin may also be effective both in the prevention of diabetes mellitus and in attenuating the associated complications, particularly cardiovascular complications [41]. Recently, it has been demonstrated that curcumin has a high affinity with protease and can be considered as an effective Covid-19 anti-protease drug [42]. Both epidemiological and experimental studies have established a favorable correlation between amelioration of heavy metal toxicity and application of curcumin [43,44]. However, a major caveat in applying curcumin is its relatively low absorption and water solubility, which considerably limits its potency. In order to enhance rapid absorption, SNEC30 has been formulated with self nano-emulsifying drug delivery system (SNEDDS) to enhance the bioavailability of curcumin, without any adverse side effects. Therefore, SNEC30 was implemented to attenuate the damage induced by arsenic on the primary and secondary immune organs in mice.

The noxious effects of ROS might be exerted at the DNA level, also known as DNA oxidation, leading to mutations and possibly cancer [6,45], at the protein level causing enzyme inhibition, denaturation and protein degradation, and at the lipid level leading to lipid peroxidation. Keeping in line with previous studies, our results indicated a sharp rise in cellular ROS in the thymus and spleen upon arsenic treatment. Activities of antioxidant enzymes, such as CAT and SOD, which are known to be the first line of defense and protect biological molecules from oxidative stress [46], have been shown to reduce significantly in response to arsenic treatment. In addition, GSH levels were also depleted after arsenic treatment, indicating thiol attenuation. These special markers have been proven to be authentic in the diagnosis of arsenic-related organ toxicity. Administration of SNEC30 for 14 days significantly restored the activities of these enzymes in the thymus and spleen of mice, suggesting that SNEC30 could successfully attenuate oxidative stress in $NaAsO_2$-treated mice without causing tissue damage.

Recent studies have shown that a variety of cell homeostasis mechanisms work together to reduce ROS-induced damage to cells and attempt to promote cell survival under conditions of stress. Autophagy is one of the major mechanisms maintaining cellular homeostasis [47]. ROS and autophagy play important roles in stress response in cells through a number of complicated signaling pathways [48,49]. However, if cells are severely damaged, autophagy backs out as a cell survival mechanism and drives the cells towards apoptosis either by active degradation of cellular organelles or by accelerated rate of passive non-selective degradation of cellular components, challenging cell survivability [3]. Concomitant with these reports, we have shown an increased autophagic activity in the arsenic-exposed thymus and spleen of mice, leading to accelerated p53-mediated intrinsic apoptosis. As a respite, treatment with SNEC30 was found to effectively counteract the toxic effects of sodium arsenite-induced cellular toxicity and restore structural and functional homeostasis in the experimental model. Furthermore, SNEC30 prevented the occurrence of apoptosis in the immune organs and assured overall improvement in the physiology of the mice.

5. Conclusion

Exposure to arsenic leads to a severe imbalance of general physiological conditions of an organism, including suppression of the immune system, and may culminate in life-threatening diseases. The anti-oxidant properties of SNEC30, which prevent further deterioration and reverse the damages to the immune organs, assures beneficial outcome for organisms who are inadvertently exposed to environmental and acute doses of arsenic. Amelioration by SNEC30 includes reformation of tissue architecture, decline in arsenic-induced oxidative stress by virtue of its antioxidant potential, and reduction of cell death in the thymus and spleen of Swiss albino mice. Therefore, it may be reiterated that dietary intervention and SNEC30 supplementation will help in curbing the adverse effects of arsenic in organisms. Nevertheless, a more detailed molecular evaluation of the therapeutic efficacies of this formulation will endorse efficient clinical outcome, since SNEC30 has no side effects and promotes improvement of overall health. In addition, the delivery of this nanoemulsion, either *via* oral or systemic routes, need to be delineated and justified for better efficacy of the formulation in patients. Additionally, whether SNEC30 should be used alone or in combination with other drugs which could enhance its effectiveness is a question worthy of investigation in future.

CRediT authorship contribution statement

Zarqua Jamal: Data curation, Formal analysis, Investigation, Validation, Writing - original draft, Writing - review & editing. **Joydeep Das:** Data curation, Investigation. **Payal Gupta:** Data curation. **Pubali Dhar:** Formal analysis, Resources. **Sreya Chattopadhyay:** Formal analysis, Resources. **Urmi Chatterji:** Conceptualization, Funding acquisition, Project administration, Resources, Validation, Writing - review & editing.

Declaration of Competing Interest

The authors declare that they have no known competing financial interests or personal relationships that could have appeared to influence the work reported in this paper.

Acknowledgements

We acknowledge the University Grants Commission (UGC), Government of India, for grant to U.C. and fellowship support to Z.J. We would also like to acknowledge the Central Instrument Facility of CRNN (University of Calcutta) for providing flow cytometry and SEM facilities. We are also thankful to DST-FIST, UGC-SAP and DST-PURSE for infrastructure support.

Appendix A. Supplementary data

Supplementary material related to this article can be found, in the online version, at doi:https://doi.org/10.1016/j.toxrep.2021.07.010.

References

[1] P.B. Tchounwou, C.G. Yedjou, A.K. Patlolla, D.J. Sutton, Heavy metal toxicity and the environment, J. Exp. Zool. Suppl. 101 (2014) 133–164, https://doi.org/10.1007/978-3-7643-8340-4_6.

[2] Q. Zhou, Y. Gu, X. Yue, G. Mao, Y. Wang, H. Su, et al., Combined toxicity and underlying mechanisms of a mixture of eight heavy metals, Mol. Med. Rep. 15 (2017) 859–866, https://doi.org/10.3892/mmr.2016.6089.

[3] Z. Jamal, J. Das, S. Ghosh, A. Gupta, S. Chattopadhyay, U. Chatterji, Arsenic-induced immunomodulatory effects disorient the survival-death interface by stabilizing the Hsp90/Beclin1 interaction, Chemosphere 238 (2019) 124647, https://doi.org/10.1016/j.chemosphere.2019.124647.

[4] H. Zhao, Y. Wang, M. Guo, D. Fei, M. Mu, H. Yu, et al., Hepatoprotective effects of zinc (II) via cytochrome P-450/reactive oxygen species and canonical apoptosis pathways after arsenite waterborne exposure in common carp, Chemosphere 236 (2019), 124869, https://doi.org/10.1016/j.chemosphere.2019.124869.

[5] Q. Tang, L. Bai, Z. Zou, P. Meng, Y. Xia, S. Cheng, et al., Ferroptosis is newly characterized form of neuronal cell death in response to arsenite exposure, Neurotoxicology 67 (2018) 27–36, https://doi.org/10.1016/j.neuro.2018.04.012.

[6] A. Chatterjee, U. Chatterji, All Trans retinoic acid ameliorates arsenic induced oxidative stress and apoptosis in the rat uterus by modulating MAPK signaling proteins, J. Cell. Biochem. 118 (2017) 3796–3809, https://doi.org/10.1002/jcb.26029.

[7] C.J. Chen, C.W. Chen, M.M. Wu, T.L. Kuo, Cancer potential in liver, lung, bladder and kidney due to ingested inorganic arsenic in drinking water, Br. J. Cancer 66 (1992) 888–892, https://doi.org/10.1038/bjc.1992.380.

[8] C.H. Tseng, C.K. Chong, C.P. Tseng, Y.M. Hsueh, H.Y. Chiou, C.C. Tseng, et al., Long-term arsenic exposure and ischemic heart disease in arseniasis-hyperendemic villages in Taiwan, Toxicol. Lett. 137 (2003) 15–21, https://doi.org/10.1016/s0378-4274(02)00377-6.

[9] A. Chatterjee, U. Chatterji, Arsenic abrogates the estrogen-signaling pathway in the rat uterus, Reprod. Biol. Endocrinol. 8 (2010) 80, https://doi.org/10.1186/1477-7827-8-80.

[10] A. Chatterjee, U. Chatterji, All-trans retinoic acid protects against arsenic-induced uterine toxicity in female Sprague-Dawley rats, Toxicol. Appl. Pharmacol. 257 (2011) 250–263, https://doi.org/10.1016/j.taap.2011.09.011.

[11] M. Argos, L. Tong, S. Roy, M. Sabarinathan, A. Ahmed, M.T. Islam, et al., Screening for gene-environment (G×E) interaction using omics data from exposed individuals: an application to gene-arsenic interaction, Mamm. Genome 29 (2018) 101–111, https://doi.org/10.1007/s00335-018-9737-8.

[12] K. Jomova, Z. Jenisova, M. Feszterova, S. Baros, J. Liska, D. Hudecova, et al., Arsenic: toxicity, oxidative stress and human disease, J. Appl. Toxicol. 31 (2011) 95–107, https://doi.org/10.1002/jat.1649.

[13] K.A. Francesconi, Arsenic species in seafood: origin and human health implications, Pure Appl. Chem. 82 (2010) 373–381, https://doi.org/10.1351/PAC-CON-09-07-01.

[14] M. Molin, S.M. Ulven, H.M. Meltzer, J. Alexander, Arsenic in the human food chain, biotransformation and toxicology–Review focusing on seafood arsenic, J. Trace Elem. Med. Biol. 31 (2015) 249–259, https://doi.org/10.1016/j.jtemb.2015.01.010.

[15] S. Gao, X. Duan, X. Wang, D. Dong, D. Liu, X. Li, et al., Curcumin attenuates arsenic induced hepatic injuries and oxidative stress in experimental mice through activation of Nrf2 pathway, promotion of arsenic methylation and urinary excretion, Food Chem. Toxicol. 59 (2013) 739–747, https://doi.org/10.1016/j.fct.2013.07.032.

[16] A.O. Abolaji, K.D. Fasae, C.E. Iwezor, M. Aschner, E.O. Farombi, Curcumin attenuates copper-induced oxidative stress and neurotoxicity in *Drosophila melanogaster*, Toxicol. Rep. 7 (2020) 261–268, https://doi.org/10.1016/j.toxrep.2020.01.015.

[17] M. Suzuki, T. Betsuyaku, Y. Ito, K. Nagai, N. Odajima, C. Moriyama, et al., Curcumin attenuates elastase- and cigarette smoke-induced pulmonary emphysema in mice, Am. J. Physiol. Lung Cell Mol. Physiol. 296 (2009) L614–23, https://doi.org/10.1152/ajplung.90443.2008.

[18] B. Salehi, P. Lopez-Jornet, E.P. López, D. Calina, M. Sharifi-Rad, K. Ramírez-Alarcón, et al., Plant-derived bioactives in oral mucosal lesions: a key emphasis to curcumin, lycopene, chamomile, *Aloe vera*, green tea and coffee properties, Biomolecules 9 (2019) 106, https://doi.org/10.3390/biom9030106.

[19] M. Hashemzaei, K. Tabrizian, Z. Alizadeh, S. Pasandideh, R. Rezaee, C. Mamoulakis, Resveratrol, curcumin and gallic acid attenuate glyoxal-induced damage to rat renal cells, Toxicol. Rep. 7 (2020) 1571–1577, https://doi.org/10.1016/j.toxrep.2020.11.008.

[20] S. Shishodia, G. Sethi, B.B. Aggarwal, Curcumin: getting back to the roots, Ann. N. Y. Acad. Sci. 1056 (2005) 206–217, https://doi.org/10.1196/annals.1352.010.

[21] B.B. Aggarwal, S.C. Gupta, B. Sung, Curcumin: an orally bioavailable blocker of TNF and other pro-inflammatory biomarkers, Br. J. Pharmacol. 169 (2013) 1672–1692, https://doi.org/10.1111/bph.12131.

[22] K. Hede, Chinese folk treatment reveals power of arsenic to treat cancer, new studies under way, J. Natl. Cancer Inst. 99 (2007) 667–668, https://doi.org/10.1093/jnci/djk191.

[23] H. Hatcher, R. Planalp, J. Cho, F.M. Torti, S.V. Torti, Curcumin: from ancient medicine to current clinical trials, Cell. Mol. Life Sci. 65 (2008) 1631–1652, https://doi.org/10.1007/s00018-008-7452-4.

[24] V. Krup, L. Hedge Prakash, A. Harini, Pharmacological activities of turmeric (Curcuma longa linn): a Review, J. Homeop. Ayurv. Med. 2 (2013) 133, https://doi.org/10.4172/2167-1206.1000133.

[25] F.M. El-Demerdash, M.I. Yousef, F.M. Radwan, Ameliorating effect of curcumin on sodium arsenite-induced oxidative damage and lipid peroxidation in different rat organs, Food Chem. Toxicol. 47 (2009) 249–254, https://doi.org/10.1016/j.fct.2008.11.013.

[26] W.H. Chan, H.J. Wu, Protective effects of curcumin on methylglyoxal induced oxidative DNA damage and cell injury in human mononuclear cells, Acta Pharmacol. Sin. 27 (2006) 1192–1198, https://doi.org/10.1111/j.1745-7254.2006.00374.x.

[27] S. Prasad, A.K. Tyagi, B.B. Aggarwal, Recent developments in delivery, bioavailability, absorption and metabolism of curcumin: the golden pigment from golden spice, Cancer Res. Treat. 46 (2014) 2–18, https://doi.org/10.4143/crt.2014.46.1.2.

[28] B. Salehi, D. Calina, A.O. Docea, N. Koirala, S. Aryal, D. Lombardo, L. Pasqua, et al., Curcumin's nanomedicine formulations for therapeutic application in neurological diseases, J. Clin. Med. 9 (2020) 430, https://doi.org/10.3390/jcm9020430.

[29] N. Ghalandarlaki, A.M. Alizadeh, Nanotechnology-applied curcumin for different diseases therapy, Biomed Res. Int. 2014 (2014), https://doi.org/10.1155/2014/394264, 394264.

[30] K. Maiti, K. Mukherjee, A. Gantait, B.P. Saha, P.K. Mukherjee, et al., Curcumin-phospholipid complex: Preparation, therapeutic evaluation and pharmacokinetic study in rats, Int. J. Pharm. 330 (2007) 155–163, https://doi.org/10.1016/j.ijpharm.2006.09.025.

[31] M. Chakraborty, A. Mukherjee, K.M. Ahmed, A review of groundwater arsenic in the Bengal Basin, Bangladesh and India: from source to sink, Curr. Pollut. Rep. 1 (2015) 220–247, https://doi.org/10.1007/s40726-015-0022-0.

[32] A. Basu, P. Sen, A. Jha, Environmental arsenic toxicity in West Bengal, India: a brief policy review, Indian J. Public Health 59 (2015) 295–298, https://doi.org/10.4103/0019-557x.169659.

[33] E. Shaji, M. Santosh, K.V. Sarath, P. Prakash, V. Deepchand, B.V. Divya, Arsenic contamination of groundwater: a global synopsis with focus on the Indian Peninsula, Geosci. Front. (2020), https://doi.org/10.1016/j.gsf.2020.08.015.

[34] S. Choudhury, P. Gupta, S. Ghosh, S. Mukherjee, P. Chakraborty, U. Chatterji, et al., Arsenic-induced dose-dependent modulation of the NF-κB/IL-6 axis in thymocytes triggers differential immune responses, Toxicology 357-358 (2016) 85–96, https://doi.org/10.1016/j.tox.2016.06.005.

[35] D.J. Jollow, J.R. Mitchell, N. Zampaglione, J.R. Gillette, Bromobenzene-induced liver necrosis. Protective role of glutathione and evidence for 3, 4-bromobenzene oxide as the hepatotoxic metabolite, Pharmacology 11 (1974) 151–169, https://doi.org/10.1159/000136485.

[36] A. Claiborne, Catalase Activity, vol. 1, CRC Press, Boca Raton FL, 1985, pp. 283–284.

[37] S. Marklund, G. Marklund, Involvement of superoxide anion radical in the autoxidation of pyrogallol and a convenient assay for superoxide dismutase, Eur. J. Biochem. 47 (1974) 469–474, https://doi.org/10.1111/j.1432-1033.1974.tb03714.x.

[38] S.C.J. Chueh, M.K. Lai, I.S. Liu, F.C. Teng, J. Chen, Curcumin enhances the immunosuppressive activity of cyclosporine in rat cardiac allografts and in mixed lymphocyte reactions, Transplant. Proc. 35 (2003) 1603–1605, https://doi.org/10.1016/s0041-1345(03)00377-4.

[39] S. Sharma, K. Chopra, S.K. Kulkarni, J.N. Agrewala, Resveratrol and curcumin suppress immune response through CD28/CTLA-4 and CD80 co-stimulatory pathway, Clin. Exp. Immunol. 147 (2007) 155–163, https://doi.org/10.1111/j.1365-2249.2006.03257.x.

[40] A.C. Bharti, A. Panigrahi, P.K. Sharma, N. Gupta, R. Kumar, S. Shukla, et al., Clinical relevance of curcumin-induced immunosuppression in living-related donor renal transplant: an in vitro analysis, Exp. Clin. Transplant. 8 (2010) 161–171.

[41] D. Margină, O.T. Olaru, M. Ilie, D. Grădinaru, C. Guțu, S. Voicu, A. Dinischiotu, D. A. Spandidos, A.M. Tsatsakis, Assessment of the potential health benefits of certain total extracts from Vitis vinifera, Aesculus hyppocastanum and Curcuma longa, Exp. Ther. Med. 10 (2015) 1681–1688, https://doi.org/10.3892/etm.2015.2724.

[42] N. Mohammadi, N. Shaghaghi, Inhibitory effect of eight secondary metabolites from conventional medicinal plants on COVID_19 virus protease by molecular docking analysis, ChemRxiv (2020), https://doi.org/10.26434/chemrxiv.11987475.v1. Preprint.

[43] S. Daniel, J.L. Limson, A. Dairam, G.M. Watkins, S. Daya, Through metal binding, curcumin protects against lead- and cadmium-induced lipid peroxidation in rat brain homogenates and against lead-induced tissue damage in rat brain, J. Inorg. Biochem. 98 (2004) 266–275, https://doi.org/10.1016/j.jinorgbio.2003.10.014.

[44] W.R. García-Niño, J. Pedraza-Chaverrí, Protective effect of curcumin against heavy metals-induced liver damage, Food Chem. Toxicol. 69 (2014) 182–201, https://doi.org/10.1016/j.fct.2014.04.016.

[45] L. Benbrahim-Tallaa, R.A. Waterland, M. Styblo, W.E. Achanzar, M.M. Webber, M. P. Waalkes, Molecular events associated with arsenic-induced malignant transformation of human prostatic epithelial cells: aberrant genomic DNA methylation and K-ras oncogene activation, Toxicol. Appl. Pharmacol. 206 (2005) 288–298, https://doi.org/10.1016/j.taap.2004.11.017.

[46] M.K. Singh, S.S. Yadav, V. Gupta, S. Khattri, Immunomodulatory role of Emblica officinalis in arsenic induced oxidative damage and apoptosis in thymocytes of mice, BMC Complement. Altern. Med. 13 (2013) 193, https://doi.org/10.1186/1472-6882-13-193.

[47] Y. Xu, S.O. Kim, Y. Li, J. Han, Autophagy contributes to caspase-independent macrophage cell death, J. Biol. Chem. 281 (2006) 19179–19187, https://doi.org/10.1074/jbc.M513377200.

[48] B.R. Underwood, S. Imarisio, A. Fleming, C. Rose, G. Krishna, P. Heard, et al., Antioxidants can inhibit basal autophagy and enhance neurodegeneration in models of polyglutamine disease, Hum. Mol. Genet. 19 (2010) 3413–3429, https://doi.org/10.1093/hmg/ddq253.

[49] G. Filomeni, D.D. Zio, F. Cecconi, Oxidative stress and autophagy: the clash between damage and metabolic needs, Cell Death Differ. 22 (2014) 377–388, https://doi.org/10.1038/cdd.2014.150.